RSC Advances

PAPER

View Article Online
View Journal | View Issue



Cite this: *RSC Adv.*, 2016, **6**, 21725

# Europium-doped $NaYF_4$ nanoparticles cause the necrosis of primary mouse bone marrow stromal cells through lysosome damage†

Kun Ge,[ab] Wentong Sun,[a] Shaohan Zhang,[a] Shuxian Wang,*[b] Guang Jia,[a] Cuimiao Zhang[a] and Jinchao Zhang*[a]

Applications of europium-doped $NaYF_4$ ($NaYF_4$:$Eu^{3+}$) nanoparticles in biomedical fields will inevitably increase their exposure to humans, therefore, the assessment of toxicities must be taken into consideration. It was reported that $NaYF_4$:$Eu^{3+}$ nanoparticles could accumulate in the bone. However, the potential effect of $NaYF_4$:$Eu^{3+}$ nanoparticles on bone marrow stromal cells (BMSCs) has not been reported. In this study, $NaYF_4$:$Eu^{3+}$ particles with diameters of 50 and 200 nm (NY50 and NY200) were prepared and characterized by scanning electron microscopy, transmission electron microscopy, powder X-ray diffraction, photoluminescence excitation and emission spectra, and dynamic light scattering. The cytotoxicity of $NaYF_4$:$Eu^{3+}$ particles on BMSCs and the associated mechanisms were further studied. The results indicated that $NaYF_4$:$Eu^{3+}$ particles could be uptaken into BMSCs and primarily localized in the lysosome. $NaYF_4$:$Eu^{3+}$ particles effectively inhibited the viability of BMSCs in a size-dependent manner at 24 and 48 h. After cells were treated with 20 μg $mL^{-1}$ of NY50 and NY200 for 24 h, $NaYF_4$:$Eu^{3+}$ particles could trigger cell necrosis in a size-dependent manner. The percentage of necrotic BMSCs ($PI^+$/Annexin $V^-$) increased to 15.93 and 14.73%. Necrosis was further verified by increased lactate dehydrogenase leakage. Meanwhile, both NY50 and NY200 induced an increased cell population in the S and G2/M phases. The following mechanism is involved in $NaYF_4$:$Eu^{3+}$ particle-induced BMSCs necrosis: the $NaYF_4$:$Eu^{3+}$ particles lead to lysosomal rupture by lysosomal swelling, permeabilization of lysosomal membranes, and increased cathepsins B and D. In addition, $NaYF_4$:$Eu^{3+}$ particle-induced BMSCs necrosis is also directly caused by the overproduction of ROS through injury to the mitochondria. This study provides novel evidence to elucidate the toxicity mechanisms for bone metabolism and may be beneficial to more rational applications of these nanomaterials in the future.

Received 19th January 2016
Accepted 5th February 2016

DOI: 10.1039/c6ra01625a

www.rsc.org/advances



## Introduction

At present, rare earth-based nanomaterials have been widely used in biomedical fields due to their unique physicochemical properties. Rare earth fluoride compounds have attracted special interest in luminescence applications. In particular, $NaYF_4$ is considered to be one of the most efficient host materials for upconversion phosphors when it is doped with rare earth ions. Kumar *et al.* synthesized 20–30 nm $Eu^{3+}$, $Er^{3+}$, $Yb^{3+}$, and $Gd^{3+}$ co-doped $NaYF_4$ nanocrystals, and these nanocrystals were further functionalized by conjugating with tumor-specific antibodies. They found that the upconversion nanophosphors ($NaYF_4$:$Er^{3+}$,$Yb^{3+}$) demonstrated some advantages for *in vitro* imaging of cancer cells and *in vivo* imaging in tissues.[1] Shen *et al.* reported that the multishell structured nanoprobe ($NaYF_4$:Yb/Tm@$NaLuF_4$@$NaYF_4$@$NaGdF_4$) displayed great potential for *in vivo* upconversion luminescence, X-ray computed tomography, and magnetic resonance trimodal imaging. In addition, it also showed great potential for *in vivo* targeted upconversion luminescence imaging of tumor-bearing mice.[2] Hou *et al.* prepared a novel multifunctional dual drug delivery system based on poly(ε-caprolactone)-gelatin encapsulating $NaYF_4$:$Yb^{3+}$,$Er^{3+}$@$mSiO_2$ nanoparticles electrospun composite fibers. This system can offer site-specific dual drug delivery to lesions of the body and demonstrate potential application in wound healing or implant in surgery.[3] Yet, despite of such interest, more wide-scale biomedical applications have been limited largely due to an absence of a thorough toxicity evaluation. So the level of risk of these rare earth fluoride nanomaterials to the general public must be taken into consideration.

[a]*Key Laboratory of Chemical Biology of Hebei Province, Key Laboratory of Medicinal Chemistry and Molecular Diagnosis of the Ministry of Education, College of Chemistry & Environmental Science, Hebei University, Baoding 071002, P. R. China. E-mail: 13832200993@163.com; jczhang6970@163.com; Tel: +86-312-5079627*

[b]*Affiliated Hospital of Hebei University, Baoding 071000, P. R. China*

† Electronic supplementary information (ESI) available. See DOI: 10.1039/c6ra01625a

It was reported that β-$NaYF_4$:Ce,Tb nanophosphors showed toxic effects at sufficiently high concentration *in vitro* and *in vivo*.[4] The core–shell structured nanocrystals silica/$NaYF_4$ demonstrated good biocompatibility *in vitro* and *in vivo*. Both skeletal myoblasts and bone marrow stromal cells (BMSCs) could survive well even at the highest concentration. The lung and the heart are two target organs. However, they could be mostly cleared after day 7 post-injection.[5] Toxicity studies of polyacrylic acid (PAA)-coated upconversion nanophosphors $NaYF_4$:Yb,Tm (PAA-UCNPs) have been reported. The results demonstrated that mice could survive for 115 days without any apparent adverse effects by intravenous injection with 15 mg $kg^{-1}$ of PAA-UCNPs. In addition, no overt toxicity of PAA-UCNPs in mice at long exposure was observed.[6] Chen *et al.* reported that europium doped $NaYF_4$ particles displayed size-dependent cytotoxicity for endothelial cells, the damage pathway may be related to the reactive oxygen species (ROS) generation and mitochondrial damage.[7] The biodistribution experiment showed that fluorine-18 labeled $NaYF_4$ nanoparticles could accumulate in the bone tissue.[8] However, to the best our knowledge, the effect of $NaYF_4$:$Eu^{3+}$ particles on bone metabolism has not been reported.

It is well-known that BMSCs are multipotent stromal cells. As a cell model, BMSCs have attracted particular attention in stem cell therapy and tissue engineering fields because they can be readily isolated and expanded *ex vivo* and induced either *in vitro* or *in vivo* to terminally differentiate into osteoblasts, chondrocytes, adipocytes, *etc.*[9] Ma *et al.* used BMSCs to evaluate cytotoxicity of electrospun porous YAG:$Nd^{3+}$ fibers employed in luminescent drug carriers. The results revealed that these YAG:$Nd^{3+}$ fibers were biocompatible.[10] Liu *et al.* reported that carboxylated carbon nanotubes could inhibit the proliferation and osteogenic differentiation of BMSCs through a Smad-dependent bone morphogenetic protein signaling pathway.[11] Yang *et al.* found that metallofullerene nanoparticles could promote osteogenic differentiation of BMSCs through BMP signaling pathway, moreover, effectively improve bone density and prevent osteoporosis *in vivo*.[12] Up to now, the effects of $NaYF_4$:$Eu^{3+}$ particles on BMSCs have not been reported. In this study, we prepared $NaYF_4$:$Eu^{3+}$ particles (50 nm and 200 nm) and used primary mouse BMSCs as a cell model to investigate the cytotoxicity of $NaYF_4$:$Eu^{3+}$ particles on BMSCs and the associated mechanisms for the first time.

# Materials and methods

## Materials

4–6 week ICR mice were purchased from Beijing Vitalriver Experimental Animal Technology Co. Ltd. All experiments were performed in compliance with the relevant laws and institutional guidelines, and also state that the Administration Office Committee of Laboratory Animal has approved the experiments. Dulbecco's modified Eagle's medium (DMEM), fatal bovine serum (FBS), and trypsin were obtained from Gibco (Grand Island, NY, USA). 3-(4,5-Dimethylthiazol-2-yl)-2,5-diphenyl tetrazolium bromide (MTT), propidium iodide (PI), and acridine orange (AO) were purchased from Sigma-Aldrich (St. Louis, MO, USA). 2′,7′-Dichlorofluorescin diacetate (DCFH-DA), rhodamine 123 (RH123), LysoTracker Red, LysoTracker Green and MitoTracker Green were purchased from Invitrogen (Lifetechnologies, USA). Lactate dehydrogenase (LDH) release kit and Annexin V-FITC apoptosis detection kit were obtained from Beyotime Institute of Biotechnology (Jiangsu, China). Cathepsin B, cathepsin D, Bax, and Bid ELISA detection kits were purchased from Ha Ling Sheng Wu (Shanghai, China). RIPA lysis buffer were obtained from BestBio (Shanghai, China).

The chemicals $Y_2O_3$ and $Eu_2O_3$ with purity of 99.99% were obtained from Aladdin (Shanghai, China). $Y(NO_3)_3$ and $Eu(NO_3)_3$ solutions with concentration of 1.0 M and 0.1 M were prepared by dissolving the $Y_2O_3$ and $Eu_2O_3$ in dilute nitric acid at an elevated temperature, respectively. All the chemical agents were analytical grade.

## Preparation of $NaYF_4$:$Eu^{3+}$ particles

$NaYF_4$:$Eu^{3+}$ particles with size of 50 nm (labeled as NY50) were prepared by a hydrothermal route.[13] In brief, 1 mL of $Eu(NO_3)_3$ (0.1 M), 1.9 mL of $Y(NO_3)_3$ (1.0 M), and 4 mmol of trisodium citrate were mixed in a 20 mL ethylene glycol (EG, 99%) solvent to form a transparent solution. Then, 3 mmol of $NaBF_4$ was added to 8 mL $H_2O$ to form the aqueous solution. Afterward, the above two solutions were mixed together. After being vigorously stirred for 15 min, the mixtures were transferred into a 50 mL Teflon bottle which was held in a stainless steel autoclave, sealed, and maintained at 180 °C for 2 h. When the autoclave was cooled to room temperature naturally, the obtained precipitate was separated by centrifugation, washed with deionized water and ethanol for several times. Finally, the product was dried in air at 70 °C for 12 h to obtain the $NaYF_4$:$Eu^{3+}$ particles.

$NaYF_4$:$Eu^{3+}$ particles with size of 200 nm (labeled as NY200) were prepared according to the literature.[14,15] An aqueous solution of $Eu(NO_3)_3$ and $Y(NO_3)_3$ (total molar is 0.7 mmol, molar ratio: Y/Eu = 98 : 2) was mixed with a 25 mL aqueous solution of ethylenediamine tetraacetic acid disodium salt (EDTA) under vigorous magnetic stirring. Then, 10 mL of NaF aqueous solution (the molar ratio of lanthanide/EDTA/NaF is 1/1/12) was added into the above solution and stirred for 1 h. The mixing solution was transferred into a 50 mL autoclave which was sealed, and maintained at 180 °C for 2 h, then cooled to room temperature naturally. The resulting white precipitate was separated by centrifugation, washed with deionized water and ethanol for several times. Finally, the product was dried in air to obtain the final $NaYF_4$:$Eu^{3+}$ sample.

## Characterization of $NaYF_4$:$Eu^{3+}$ particles

The morphology and structure of the $NaYF_4$:$Eu^{3+}$ particles was characterized by scanning electron microscope (SEM) (JEOL, JSM-7500F, JPN) and transmission electron microscopy (TEM) (Tecnai G2, S-Twin, FEI). The $NaYF_4$:$Eu^{3+}$ particles were characterized by X-ray diffractometer (XRD) (Bruker, D8 Advance, GER) equipped with a rotation anode CuKα radiation in the range of 20–80° in steps of 0.02° for the determination of crystal structure and phase. The excitation and emission spectra were

 

record on a spectrophotometer (Hitachi, F-4500 FL, JPN) with a Xenon lamp as the excitation source at room temperature. The size distribution of the $NaYF_4$:$Eu^{3+}$ particles in culture condition was evaluated by dynamic light scattering (DLS) (Beckman Coulter, Delsa Nano C, USA).

### Isolation and culture of primary BMSCs

The mouse primary BMSCs were obtained from 4–6 week ICR mice.[16] In brief, mice were executed by cervical vertebra, femora and tibiae were aseptically harvested, and the whole bone marrow was flushed by supplemented DMEM in a 1 mL syringe and a 25 gauge needle. Cells were maintained in DMEM supplemented with 10% FBS and 100 U $mL^{-1}$ penicillin-streptomycin in a humidified atmosphere of 5% $CO_2$ at 37 °C. The medium was replaced every 3 d in all experiments, the nonadherent cells were removed by fresh DMEM.

### Cell viability assay

MTT assay was used to detect the viability of BMSCs treated with $NaYF_4$:$Eu^{3+}$ particles.[17] Briefly, BMSCs ($1 \times 10^5$ cells per well) were seeded in 96 well culture plates and cultured at 37 °C in a 5% $CO_2$ humidified incubator overnight. NY50 and NY200 were added to wells at final concentrations of 10, 20, 40, 60, and 80 μg $mL^{-1}$. Control group was prepared by addition of DMEM, and blank group was set by addition of DMEM without cells. After treatment for 24, and 48 h, MTT solution (5.0 mg $mL^{-1}$) was added and incubated for 4 h at 37 °C. The supernatant was removed and 100 μL dimethylsulfoxide (DMSO) was added to the wells. The optical density (OD) value was read at a wavelength of 570 nm by a microplate reader (Molecular Devices, VersaMax, USA). The cell viability (%) was calculated according to the formula: $(OD_{treated} - OD_{blank})/(OD_{control} - OD_{blank}) \times 100$.

### Uptake studies

The uptake studies were performed by flow cytometry.[18] In brief, BMSCs were seeded in six-well plates at $5 \times 10^6$ cells per well and cultured overnight. Then the cells were treated with NY50 and NY200 at a concentration of 20 μg $mL^{-1}$ for 4 h. Then the cells were washed three times with 0.01 M phosphate-buffered saline (PBS), digested by trypsin solution, and resuspended in PBS. The uptake of particles was analyzed by a FACScalibur flow cytometer (Becton Dickinson, USA) and the side scatter data were analyzed using CELLQuest 6.0 software.

### Subcellular localization

The subcellular localization of NY50 and NY200 in BMSCs was studied according to the literature as described by Chen *et al.*[7] In brief, cells were seeded on a 30 mm cell culture coverlips at $2.5 \times 10^6$ cells per well and cultured for 4 days. Then cells were incubated with NY50 and NY200 at a concentration of 20 μg $mL^{-1}$ for 4 h. After that, cells were treated with LysoTracker Red (100 nmol $L^{-1}$) and MitoTracker Green (100 nmol $L^{-1}$) for 30 min, then washed with PBS three times. Afterwards, the intracellular localization was detected by a confocal laser microscope (Olympus, IX81, JPN). Fluorescence from $NaYF_4$:$Eu^{3+}$ particles, LysoTracker Red and MitoTracker Green was excited at 405, 559 and 488 nm, respectively.

### Annexin V/PI assay

The cell apoptosis or necrosis was measured by Annexin V-FITC/PI assay as described by Aubry *et al.*[19] Briefly, BMSCs were seeded in six-well plates at $5 \times 10^6$ cells per well and incubated for 4 days. After treatment by NY50 and NY200 at a concentration of 20 μg $mL^{-1}$ for 24 h, cells were harvested and centrifuged at $1000 \times g$ for 5 min. Then 100 μL cell suspension was mixed with 5 μL Annexin V-FITC and 5 μL PI, and further incubated in the dark at room temperature for 15 min. The fluorescence intensity of Annexin V-FITC was analyzed at an excitation/emission wavelength of 488/530 nm, PI fluorescence analysis was performed at an excitation/emission wavelength of 488/617 nm by FACScalibur flow cytometer, respectively. The data were analyzed by CELLQuest 6.0 software.

### Measurement of LDH

LDH in culture supernatant was measured using a LDH assay kit.[20] Briefly, BMCSs were seeded in 96 well plates at $1 \times 10^5$ cells per well and incubated for 4 days. Then NY50 and NY200 with a concentration of 20 μg $mL^{-1}$ were added to culture medium. After 24 h treatment, the plates were centrifuged at 400*g* for 5 min, 60 μL cell-free supernatant was incubated with 30 μL LDH substrate solution for 30 min, and then the absorbance at 490 nm was recorded on a microplate reader (Molecular Devices Versamax, USA) with the 610 nm as a reference. The LDH release over the max (%) was calculated according to the following formula:

$$\text{LDH release (\%)} = (OD_{test} - OD_{background})/(OD_{Triton\ X\text{-}100} - OD_{background}) \times 100.$$

### Swelling of lysosome assay

Swelling of lysosome was measured as described by Liu *et al.*[21] Briefly, BMSCs were seeded in 30 mm cell culture coverlips at $2.5 \times 10^6$ cells per well at 37 °C under 5% $CO_2$. Then cells were exposed to 20 μg $mL^{-1}$ NY50 and NY200 for 24 h at 37 °C. The medium was replaced with fresh prewarmed medium containing 75 nM LysoTracker Green, and the cells were further incubated for 30 min. After being washed twice by ice-cold PBS, the cells were analyzed by confocal microscopy. Fluorescence from LysoTracker Green was excited at 488 nm.

### Lysosomal stability analysis

The lysosomal stability was assessed by using AO relocation assay.[22] In brief, BMSCs were seeded into 30 mm cell culture coverlips at $2.5 \times 10^6$ cells per well at 37 °C under 5% $CO_2$. After being treated by 20 μg $mL^{-1}$ NY50 and NY200 for 24 h at 37 °C, BMSCs were washed twice with PBS, digested by trypsin solution. BMSCs were stained with 5 mg $mL^{-1}$ AO for 15 min at 37 °C, washed and resuspended in PBS. The red fluorescence

(channel 2) of 10 000 cells was recorded on a logarithmic scale by flow cytometer. Results were expressed as means of the population fluorescence.

### Cathepsin B, cathepsin D, Bax, and Bid activity measurement assay

The activity of cathepsin B, cathepsin D, Bax, and Bid was measured using the cathepsin B, cathepsin D, Bax, and Bid ELISA detection kits. Briefly, cells were seeded in 6 well culture plates at $5 \times 10^6$ cells per well. After treatment with 20 μg $mL^{-1}$ NY50 and NY200 for 24 h, cells were washed twice with PBS, digested by trypsin solution, and resuspended in PBS. After lysed by RIPA, the lysates were centrifuged at 3000 rpm for 20 min, and the supernatant was collected. The activity of cathepsin B, cathepsin D, Bax, and Bid was measured according to the manufacturer's instruction.

### Measurement of the intracellular ROS

The level of ROS was determined by using DCFH-DA.[23] In brief, BMSCs were seeded in six well plates at $5 \times 10^6$ cells per well, incubated for 4 days and then treated with NY50 and NY200 at a concentration of 20 μg $mL^{-1}$ for 24 h. The cells were further incubated with DCFH-DA solution (6 μmol $L^{-1}$) in DMEM without serum for 30 min. Then cells were washed twice by PBS, digested with trypsin solution, and centrifuged at 1000 × *g* for 5 min, and the supernatant was discarded. The pellets were resuspended in PBS, and detected by flow cytometer. The data were analyzed by CELLQuest 6.0 software, and 10 000 events were acquired in histograms. The ROS level was expressed as the ratio of mean intensity of sample/mean intensity of control cells.

### Measurement of mitochondrial membrane potential (MMP)

The MMP was measured by RH123 dye.[24] In brief, BMSCs were seeded in six well plates at $5 \times 10^6$ cells per well and incubated for 4 days. After treatment as described above, cells were washed twice by PBS, digested by trypsin solution, and stained by RH123 (10 mmol $L^{-1}$) for 30 min in the dark at 37 °C and then analyzed using flow cytometer. Fluorescent signal intensity was examined with CELLQuest 6.0 software. For each sample, 10 000 events were collected.

### Cell cycle analysis

The cell cycle analysis was performed as described by Ferlini *et al.*[25] In brief, BMSCs were treated with NY50 and NY200 at a concentration of 20 μg $mL^{-1}$ for 24 h. Then cells were harvested and fixed by 70% ice-cold ethanol at 4 °C overnight. After being washed twice with PBS, cells were stained by a solution containing 50 μg $mL^{-1}$ of PI and 100 μg $mL^{-1}$ RNase for 30 min in the dark at room temperature. The stained cells were analyzed by the FACScalibur flow cytometer, 20 000 cells per sample were acquired in histograms and data were analyzed with Modfit 3.2 software.

### Toxicity *in vivo*

For the detailed procedures of the toxicity evaluation *in vivo*, such as coefficients of liver, spleen and kidney, biochemical assay of serum, and blood-element test, see the ESI.†

### Statistical analysis

The results are shown as mean ± standard deviation (SD), measured at least for three separate experiments. Student's *t* test was used for comparison of two means. *P* values less than 0.05 were considered statistically significant at the 95% confidence interval.

## Results

### Characterizations of $NaYF_4:Eu^{3+}$ particles

Fig. 1A shows the SEM image of NY50. It can be clearly seen that the sample consists of quasi-spherical nanoparticles with diameters about 50 nm, which can be confirmed by the TEM images (Fig. 1B and C). Fig. 1D–F show the SEM and TEM images of sample NY200. One can observe that the sample is composed of monodisperse nanospheres with diameters of about 200 nm, which are non-aggregated with narrow size distribution. The corresponding selected area electron diffraction (SAED) patterns of the samples (insets in Fig. 1C and F), taken from the two samples, show diffuse rings, indicating that $NaYF_4:Eu^{3+}$ samples are polycrystalline. Fig. 1G shows the XRD patterns of NY50 and NY200. All the diffraction peaks of the samples can be well indexed as the cubic phase of $NaYF_4$ (JCPDS no. 77-2042). No additional peak of other phases can be detected, indicating the formation of pure cubic phase of $NaYF_4$ and revealing that the $Eu^{3+}$ ions have been effectively doped into the $NaYF_4$ host lattice.

The photoluminescence (PL) properties of the $NaYF_4:Eu^{3+}$ were characterized by PL excitation and emission spectra. From the PL spectra (Fig. 1H and I), it is noted that the samples with different particle sizes exhibit the similar spectral patterns without any emission band shift. The excitation spectra consist of the characteristic absorption peaks of $Eu^{3+}$ corresponding to the direct excitation from the $Eu^{3+}$ ground state into the higher excited states of the $Eu^{3+}$ f-electrons. The dominant peak is centered at 394 nm, which can be assigned to the $^7F_{0,1}$–$^5L_6$ transitions of $Eu^{3+}$ ions. Under excitation at 394 nm, the emission spectra of the $NaYF_4:Eu^{3+}$ samples exhibits the characteristic emission peaks of $Eu^{3+}$ ions, originating from the transitions from the $^5D_0$ excited state to the $^7F_J$ ($J = 6, 5, 4, 3$) ($J = 1, 2, 3, 4$) transitions, respectively. The dominating emission centered at 594 nm corresponds to the $^5D_0$–$^7F_1$ magnetic dipole transition, which indicates that $Eu^{3+}$ ions locate in an inversion symmetry site in $NaYF_4$ matrix.

As the nanomaterials enter into the physiological environment, they may tend to form the state of aggregation. So we measured the hydrodynamic diameters of the particles by DLS. As shown in Fig. 1J and K, the calculated particle sizes from DLS are similar to those of the samples observed from the SEM and TEM, which indicates that the $NaYF_4:Eu^{3+}$ particles were not seriously aggregated when they were added into cell culture medium.

 

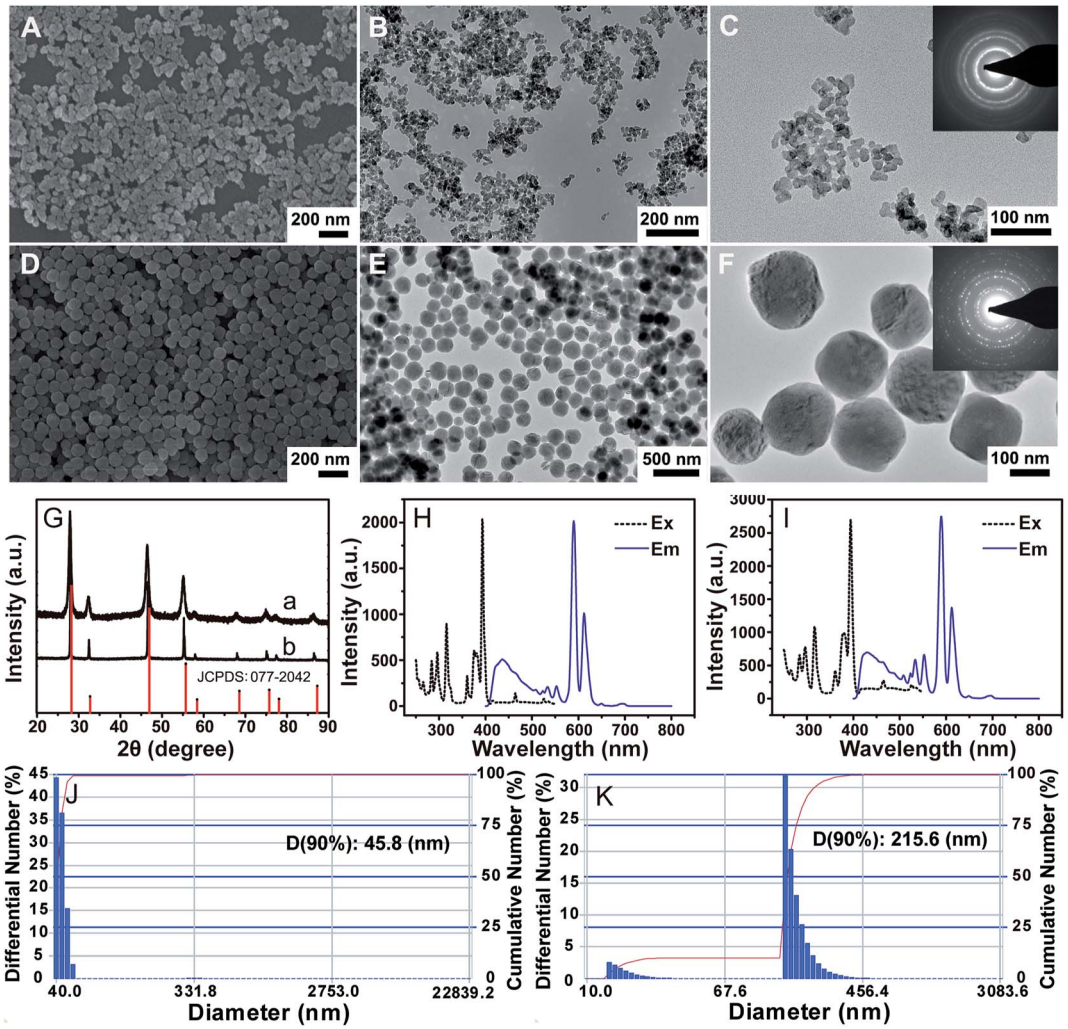


Fig. 1 Characterization of $NaYF_4:Eu^{3+}$ particles. (A and D) SEM images of NY50 (A) and NY200 (D). (B, C, E and F) TEM images of NY50 (B and C) and NY200 (E and F). Insets in (C and F) are the corresponding SAED patterns of the samples. (G) XRD patterns of NY50 and NY200. The standard data (red) of cubic $NaYF_4$ (JCPDS no. 77-2042) is presented as a reference. (H and I) PL excitation (dotted line) and emission (solid line) spectra for NY50 (H) and NY200 (I). (J and K) the DLS of NY50 (J) and NY200 (K).

### Uptake and cytotoxic effect of $NaYF_4:Eu^{3+}$ particles on BMSCs

Fig. 2A shows that NY50 and NY200 with concentration of 20 μg $mL^{-1}$ can be uptaken by BMSCs at 4 h. As shown in Fig. 2B and C, after 24 and 48 h exposure to NY50 and NY200, the viability of BMSCs was markedly decreased. The effect of NY50 and NY200 on BMSCs viability was related to the particle size at 24 h and 48 h, moreover, the smaller particles (NY50) showed greater toxicity to BMSCs.

### Subcellular location

As shown in Fig. 3, the higher co-localization signal (pink) of red fluorescence with lysosome and blue fluorescence with NY50

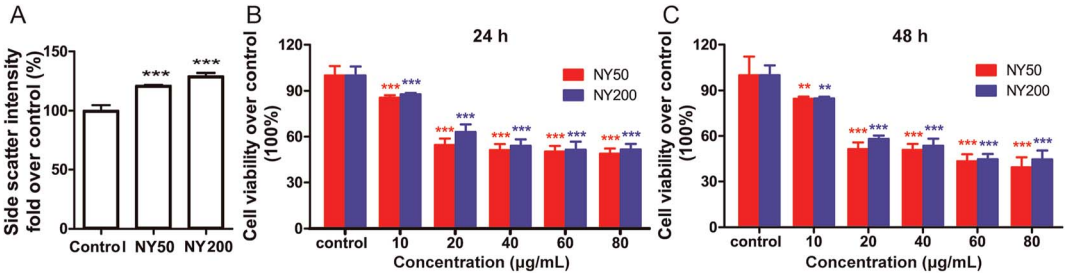


Fig. 2 The cell uptake and cytotoxicity of NY50 and NY200 for BMSCs. (A) Uptake of NY50 and NY200 by BMSCs after 4 h incubation. (B and C) The effects of NY50 and NY200 on BMSCs viability for 24 h (B) and 48 h (C). (**$P < 0.01$ and ***$P < 0.0001$ *vs.* control, $n = 3$).

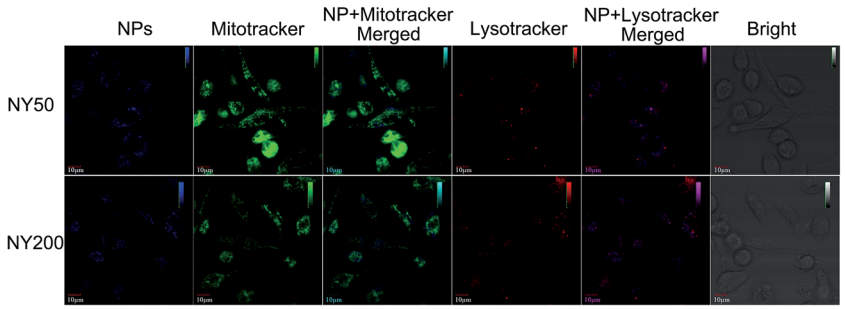


Fig. 3 Subcellular localization of NY50 and NY200 in BMSCs using laser scanning confocal microscopy.

and NY200 demonstrated that $NaYF_4:Eu^{3+}$ particles were primarily distributed in lysosome. Conversely, a very lower co-localization signal (cyan) indicated that $NaYF_4:Eu^{3+}$ particles were slightly localized in mitochondria.

### Necrotic analysis for BMSCs

The death mode of BMSCs treated with NY50 and NY200 was evaluated by flow cytometry. As shown in Fig. 4A, an apparent toxic effect of NY50 and NY200 on BMSCs could be visibly identified to be 15.93 and 14.73% of cellular necrosis ($PI^+$/Annexin $V^-$), suggesting that the cytotoxicity of NY50 and NY200 is mainly caused by the necrosis-related cell death. Meanwhile, the population of necrotic cells in NY50-treated BMSCs is more than NY200-treated BMSCs (Fig. 4B). As shown in Fig. 4C, it can be further found that NY50 and NY200 cause significant increase in the LDH release, and LDH is enhanced remarkably by NY50 treatment compared with NY200.

Both $NaYF_4:Eu^{3+}$ particles induced an increased cell population in S and G2/M phase following treatment with concentration of 20 μg $mL^{-1}$, while the percentage of cells in G0/G1 phase were declined (Fig. 4D). The results indicated that the size of particles affect the accumulation of BMSCs in the S and G2/M phase, NY50 showed an significant accumulation in S phase.

### Lysosomal lesion pathway for BMSCs

The volume of lysosome significantly increased in the NY50 and NY200-treated cells compared with that of control cells (Fig. 5A). Meanwhile, the intensity of red fluorescence in AO-exposed BMSCs was significantly decreased after NY50 and NY200-treatment compared with that of control cells (Fig. 5B), which reflects that the number of intact lysosomes has been decreased.

Intracellular ROS level in BMSCs has an approximately 1.2- and 1.1-fold increase compared with the control group after

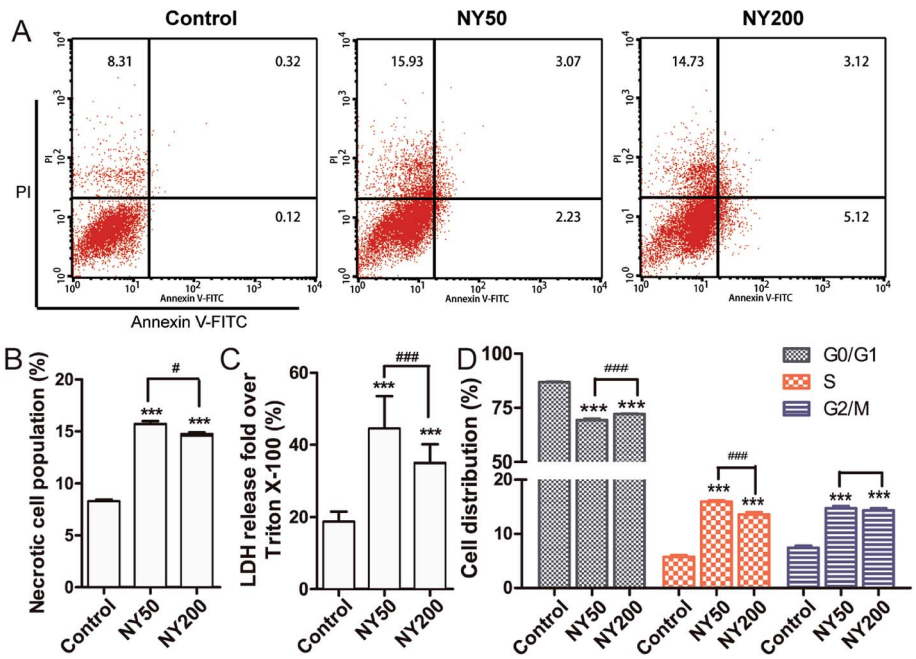


Fig. 4 (A) Evaluation of the necrosis modes of BMSCs treated with NY50 and NY200. (B) Statistic analysis of necrotic cell population. (C) LDH release in BMSCs treated with NY50 and NY200. (D) Cell cycle of BMSCs incubated with NY50 and NY200. (***$P < 0.0001$ *vs.* control, $^{\#}P < 0.05$ and $^{\#\#\#}P < 0.0001$ indicated as NY50 *vs.* NY200).

 

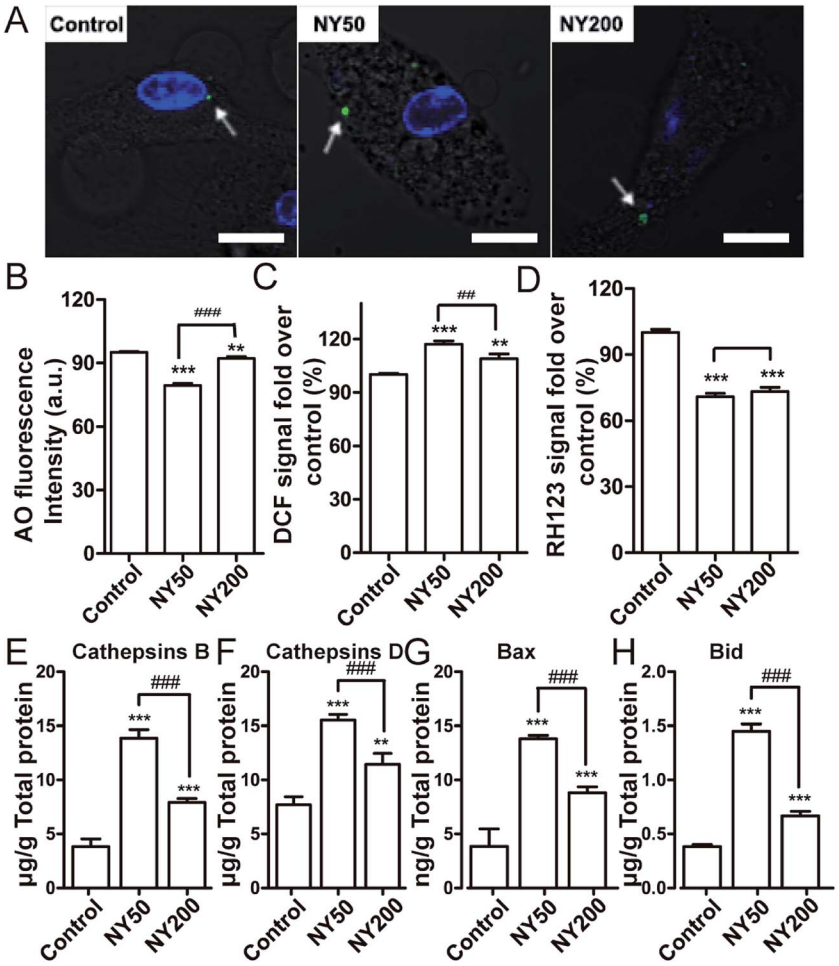


Fig. 5 Lysosomal swelling (A), lysosomal stability (B), ROS (C), MMP (D), cathepsins B level (E), cathepsins D level (F), Bax level (G) and Bid level (H) of BMSCs incubated with $NaYF_4$:$Eu^{3+}$ particles. (**$P$ < 0.01 and ***$P$ < 0.0001 *vs.* control, $^{\#\#}P$ < 0.01 and $^{\#\#\#}P$ < 0.0001 indicated as NY50 *vs.* NY200).

NY50 and NY200-treatment for 24 h (Fig. 5C), moreover, BMSCs exposed to NY50 exhibited a higher DCF fluorescence intensity in comparison with BMSCs exposed to NY200 (Fig. 5C). As shown in Fig. 5D, after incubation by $NaYF_4$:$Eu^{3+}$ particles, the MMP was dropped.

In addition, NY50 and NY200 at a concentration of 20 μg $mL^{-1}$ could notably increase the activity of cathepsin B, cathepsin D, Bax, and Bid. Meanwhile, cathepsin B, cathepsin D, Bax, and Bid value induced by NY50 have significant difference from NY200 (Fig. 5E–H).

## Discussion

Applications of nanotechnology have increased the chance of human exposure to nanomaterials, therefore, the assessment of toxicities is essential. Because the organisms are extremely complex, and it could lead to unique biological outcomes when nanostructures interact with biological components. Liu *et al.* evaluated the toxicity of $Eu^{3+}$-doped $Gd_2O_3$ ($Gd_2O_3$:$Eu^{3+}$) nanotubes in mouse. After 60 days of intraperitoneal injection, there was no significant difference of body weights between the control and all experimental groups. $Gd_2O_3$:$Eu^{3+}$ nanotubes at dose of 125 mg $kg^{-1}$ might lead to liver injury, renal toxicity, and cardiovascular damage, but $Gd_2O_3$:$Eu^{3+}$ nanotubes at dose of 12.5 mg $kg^{-1}$ and 1.25 mg $kg^{-1}$ had hardly detrimental effects on liver, kidney, and cardiovascular system.[26] Patra *et al.* reported that any significant change including the average weight loss, or adverse effects had not been observed after the administration of $Eu(OH)_3$ nanorods even at the highest dose.[27] In the present work, there was no significant difference of body weights between the control and all experimental groups (Fig. S1†). Splenomegaly, hemorrhagic ascites, abdominal adhesion and some white particulates with tunicary deposited on liver, spleen, intestine and peritoneum were observed in several mice of NY50 and NY200 high-dose groups, but no abnormal change was observed in other groups after 35 days exposure. For the coefficient of liver and kidney to body weight, there was no obvious difference between the control and all experimental groups, but the spleen in all tested groups showed higher coefficient than that of the control group (Fig. S2†). The blood biochemical tests are often used in diagnosis of diseases of liver, kidney, and cardiovascular system, and also widely used

in monitoring the response to the exogenous toxic exposure.[28] The blood biochemical tests of alanine aminotransferase (ALT), aspartate aminotransferase (AST), and alkaline phosphatase (ALP) are widely used to elevate liver function. When the liver is in dysfunction, the levels of the above enzymes will rise. The blood biochemical tests of creatine kinase (CK), lactate dehydrogenase (LDH), and alpha-hydroxybutyrate dehydrogenase (HBDH) are widely used to diagnose heart diseases. LDH test in serum is often used to diagnose heart attack, anemia, and liver diseases. In general, high LDH level shows the myocardial lesion combining with CK and HBDH levels. Their elevated levels suggest the occurrence of the ischemic heart disease, acute coronary syndromes, *etc.* The blood urea, uric acid (UA) and creatinine (Cr) are indicators for renal function. If renal function is deteriorated, the urea, UA and Cr levels will rise. Our results indicated that $NaYF_4$:$Eu^{3+}$ particles increased AST level and AST/ALT at NY50 and NY200 middle- and high-dose groups (Table S1†). The elevated levels indicated that hepatic function might be impaired. In the high-dose groups, there were no difference in the value of CK, but the HBDH and LDH levels increased obviously compared with the control group (Table S1†). In all tested groups, there was no difference for the values of urea, UA and Cr compared with the control group (Table S1†). The results indicated that the high-dose 50 nm and 200 nm $NaYF_4$:$Eu^{3+}$ particles might induce to liver injury and cardiovascular damage, and the middle-dose $NaYF_4$:$Eu^{3+}$ particles lead to liver injury, but the low-dose $NaYF_4$:$Eu^{3+}$ particles had hardly detrimental effects on liver, kidney, and cardiovascular system. For blood-elements, WBC number increased and HGB level decreased significantly in the NY50 high-dose group (Table S2†). WBC number and HGB level reflect inflammatory response and nutrient status *in vivo*, respectively, so $NaYF_4$:$Eu^{3+}$ particles might cause inflammation and anemia in the NY50 high-dose group. The results of other groups indicated that $NaYF_4$:$Eu^{3+}$ particles had hardly toxicity to hematological system.

*In vitro* experiment, the cytotoxicity indicated that $NaYF_4$:$Eu^{3+}$ particles effectively inhibited the viability of BMSCs in a size-dependent manner at 24 and 48 h (Fig. 2B and C). Annexin V/PI staining and LDH leakage assays were used to further assess the mode of cell death induced by $NaYF_4$:$Eu^{3+}$ particles.[29] In Annexin V-FITC/PI dual staining assay, we observed a significant increase in the percentage of PI positive cells after exposure to 20 μg $mL^{-1}$ of $NaYF_4$:$Eu^{3+}$ particles for 24 h (Fig. 4A and B). The results demonstrated that necrosis was the predominant cell death mode. As we know, the integrity of cell membrane was one of the most important evaluation criterions for distinguishing necrosis from apoptosis. Necrotic cells typically undergo organelle damage and plasma membrane rupture, thereby releasing intracellular components such as LDH. LDH, a stable cytosolic enzyme in normal cells, can be leaked into the extracellular fluid only after membrane damage. Therefore, the LDH release is an indicator of necrosis due to cell membrane damage. In our work, a significant increase in LDH leakage was observed after exposure to $NaYF_4$:$Eu^{3+}$ particles (Fig. 4C). The above results further confirmed that $NaYF_4$:$Eu^{3+}$ particles triggered cell death mainly by necrosis. Moreover, the percentage of necrotic cells and the concentration of released LDH in BMSCs induced by NY50 are more than NY200 (Fig. 4B and C). The degree of necrosis in BMSCs may have some relationship with the particle size of $NaYF_4$:$Eu^{3+}$ particles.

It is well known that subcellular localization pattern of nanomaterials has important effect on their toxicity.[30] Localization of nanomaterials in mitochondria and/or nucleus may severely influence cellular functions, because mitochondria and nucleus are important functional compartments of cells in cell metabolism and proliferation.[31] It was reported that $NaYF_4$ nanomaterials could induce significant cytotoxicity with entering mitochondria.[7] Our study suggests that $NaYF_4$:$Eu^{3+}$ particles (50 nm and 200 nm) were primarily distributed in lysosome and slightly localized in mitochondria (Fig. 3). Lysosomes as hydrolase-rich organelles are acidic and play a major role in intracellular protein recycling, which has been increasingly linked to cell death process.[32,33] Here, we stained the NY50- and NY200-treated cells with LysoTracker Green to examine the accumulation effect of the particles in the lysosome. LysoTracker Green is a green fluorescent dye that is used to label and track acidic organelles in live cells. AO relocation method was used to further investigate the lysosomal stability of NY50- and NY200-treated cells.[34] In our work, the accumulation of NY50 and NY200 into lysosome caused lysosomal swelling, permeabilization of lysosomal membranes, and increased cathepsins B and D (Fig. 5A, B, E and F). The larger lysosomes are easier to break down and cause cytosolic acidification, followed with degradation of cellular compartments and leading to uncontrolled cell death by necrosis.[33] Based on above analysis, we deduced that $NaYF_4$:$Eu^{3+}$ particles exhibited obvious cytotoxicity on BMSCs, and the cytotoxicity of $NaYF_4$:$Eu^{3+}$ particles might be related to lysosomes.

In more recent years, necrosis has also been recognized as a signaling- or damage-induced process of cell death, in which enhanced generation of ROS and damage of mitochondria.[33] In the present study, we found that $NaYF_4$:$Eu^{3+}$ particles increased intracellular ROS level (Fig. 5C) and decreased MMP (Fig. 5D) in BMSCs, and NY50 with smaller particle size showed more ROS production (Fig. 5C). Increased ROS level could cause lysosomal rupture and release of cathepsins, decrease MMP, and lead DNA and protein damage.[35] Mitochondria are of critical importance for the energy production of cells and particularly involved in the determination of the response to intracellular damage, meanwhile, disruption of mitochondria function could also lead to an increase in intracellular ROS.[31,36] The released cathepsins B and D from lysosomes could increase the cellular levels of Bax and Bid (Fig. 5G and H), which anchored on the surface of mitochondria membrane. The increased Bax and Bid could change MMP and further induce the intracellular ROS production. Oxidative stress in $NaYF_4$:$Eu^{3+}$ particles treated cells indicated the possibility of DNA damage where the early effect will be evidenced in cell cycle progression. BMSCs with damaged DNA accumulated in S phase (DNA synthesis) and G2/M phase (gap2/mitosis) (Fig. 4D). Absence of massive necrosis of $NaYF_4$:$Eu^{3+}$ particles accompanied by S and G2/M arrest indicated a restained mitosis and retarded cell proliferation. It has been reported that many

 

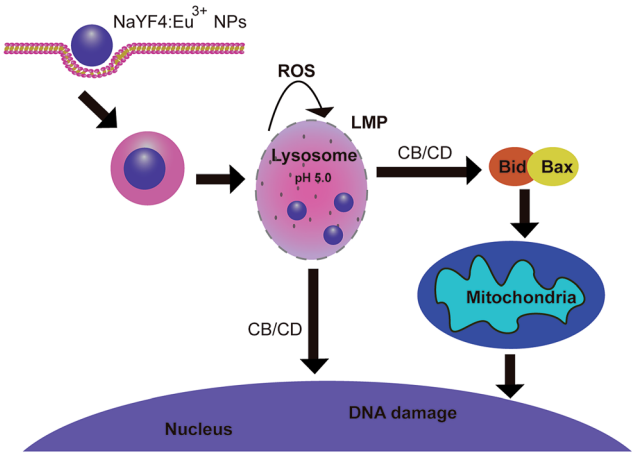


Fig. 6 The mechanism of the necrosis of BMSCs induced by $NaYF_4:Eu^{3+}$ particles. CB/CD represent cathepsins B/cathepsins D.

nanoparticles could induce cell necrosis. For example, Jiang *et al.* reported that Ag nanoparticles could induce necrosis by the increased intracellular ROS levels in CHO-K1 cell line.[31] In our previous work, we found that $Gd_2O_3:Eu^{3+}$ nanotubes could induce BMSCs necrosis through two pathways, the first is lysosomal rupture and release of cathepsins B; the another is the overproduction of ROS injury to the mitochondria and DNA.[37] In our present work, we found that $NaYF_4:Eu^{3+}$ particles could induce BMSCs necrosis through lysosomal membrane permeabilization, increase intracellular ROS, cathepsins B and D, Bax, and Bid, and damage of mitochondria and DNA. Lysosomal membrane permeabilization is a potentially lethal event because of the ectopic presence of lysosomal proteases including cathepsins B and D in the cytosol, and cathepsins B then triggers further lysosomal membrane permeabilization.[38] Altogether, cathepsins B and D may directly attack lysosomes from inside and/or outside and facilitate lysosomal membrane permeabilization-mediated cell death. Therefore it manifested that lysosomal membrane damage induced cathepsins B and D release contributed significantly to $NaYF_4:Eu^{3+}$ particles-mediated necrosis in BMSCs.

## Conclusion

On the basis of the above findings, a schematic model was proposed to describe the mechanism of the necrosis of BMSCs induced by $NaYF_4:Eu^{3+}$ particles (Fig. 6). The $NaYF_4:Eu^{3+}$ particles (50 and 200 nm) were uptaken into BMSCs and primarily localized in lysosome. The $NaYF_4:Eu^{3+}$ particles could trigger the necrosis of BMSCs. On the one hand, the $NaYF_4:Eu^{3+}$ particles could lead to lysosomal rupture which is a pathway mediating necrosis. On the other hand, $NaYF_4:Eu^{3+}$ particles-induced BMSCs necrosis is also directly caused by the overproduction of ROS through injury to the mitochondria. The results provide basic research data for constructing the biosecurity evaluation methods and standards of rare earth nanomaterials, and promoting the healthy and sustainable development of rare earth nanotechnology.

## Conflict of interest

The authors declare that no competing interests exist.

## Acknowledgements

This work was supported in part by Chinese Natural Science Foundation Project (21271059, 81200078, 21301046, 51302062), "Three Three Three" Talents Project of Hebei Province (A201401002), Research Fund for the Doctoral Program of Higher Education of China (20111301110004, 20131301120004), Hebei Province "Hundred Talents Program" (BR2-202), Key Program of Hebei Education Department (ZD2015031), China Postdoctoral Science Foundation Funded Project (2013M530119, 2014T70226), Training Program for Innovative Research Team and Leading Talent in Hebei Province University (LJRC024), Distinguished Young Scholars Fund of Hebei University (2015JQ04) and SRF for ROCS (SEM).

## References

1 R. Kumar, M. Nyk, T. Y. Ohulchanskyy, C. A. Flask and P. N. Prasad, *Adv. Funct. Mater.*, 2009, **19**, 853–859.
2 J. W. Shen, C. X. Yang, L. X. Dong, H. R. Sun, K. Gao and X. P. Yan, *Anal. Chem.*, 2013, **85**, 12166–12172. [PMID: 24237132].
3 Z. Hou, X. Li, C. Li, Y. Dai, P. Ma, X. Zhang, X. Kang, Z. Cheng and J. Lin, *Langmuir*, 2013, **29**, 9473–9482. [PMID: 23855606].
4 G. H. Jang, M. P. Hwang, S. Y. Kim, H. S. Jang and K. H. Lee, *Biomaterials*, 2014, **35**, 440–449. [PMID: 24094937].
5 R. Abdul Jalil and Y. Zhang, *Biomaterials*, 2008, **29**, 4122–4128. [PMID: 18675453].
6 L. Xiong, T. Yang, Y. Yang, C. Xu and F. Li, *Biomaterials*, 2010, **31**, 7078–7085. [PMID: 20619791].
7 S. Chen, C. Zhang, G. Jia, J. Duan, S. Wang and J. Zhang, *Mater. Sci. Eng., C*, 2014, **43**, 330–342. [PMID: 25175221].
8 Y. Sun, M. Yu, S. Liang, Y. Zhang, C. Li, T. Mou, W. Yang, X. Zhang, B. Li, C. Huang and F. Li, *Biomaterials*, 2011, **32**, 2999–3007. [PMID: 21295345].
9 R. O. Oreffo, C. Cooper, C. Mason and M. Clements, *Stem Cell Rev.*, 2005, **1**, 169–178. [PMID: 17142852].
10 Z. Ma, H. Ji, D. Tan, G. Dong, Y. Teng, J. Zhou and J. Qiu, *Chem.–Eur. J.*, 2012, **18**, 2609–2616. [PMID: 22271350].
11 D. Liu, D. Yi, D. Zhang, J. Zhang and M. Yang, *ACS Nano*, 2010, **4**, 2185–2195. [PMID: 20218664].
12 K. Yang, W. Cao, X. Hao, X. Xue, J. Zhao, J. Liu, Y. Zhao, J. Meng, B. Sun, J. Zhang and X. J. Liang, *Nanoscale*, 2013, **5**, 1205–1212. [PMID: 23299786].
13 C. Zhang, P. Ma, C. Li, G. Li, S. Huang, D. Yang, M. Shang, X. Kang and J. Lin, *J. Mater. Chem.*, 2011, **21**, 717–723.
14 X. Kang, Z. Cheng, C. Li, D. Yang, M. Shang, P. Ma, G. Li, N. Liu and J. Lin, *J. Phys. Chem. C*, 2011, **115**, 15801–15811.
15 Y. Sun, Y. Chen, L. Tian, Y. Yu, X. Kong, J. Zhao and H. Zhang, *Nanotechnology*, 2007, **18**, 275609.
16 K. A. Kelly and J. M. Gimble, *Endocrinology*, 1998, **139**, 2622–2628. [PMID: 9564879].

17 D. Zhang, C. Yi, J. Zhang, Y. Chen, X. Yao and M. Yang, *Nanotechnology*, 2007, **18**, 475102.
18 H. Suzuki, T. Toyooka and Y. Ibuki, *Environ. Sci. Technol. Libr.*, 2007, **41**, 3018–3024. [PMID: 17533873].
19 J. P. Aubry, A. Blaecke, S. Lecoanet-Henchoz, P. Jeannin, N. Herbault, G. Caron, V. Moine and J. Y. Bonnefoy, *Cytometry*, 1999, **37**, 197–204. [PMID: 10520200].
20 J. L. Williams, G. K. Fyfe, C. P. Sibley, P. N. Baker and S. L. Greenwood, *Am. J. Physiol.: Regul., Integr. Comp. Physiol.*, 2008, **295**, R1204–R1213. [PMID:18703414].
21 Y. Liu, F. Jiao, Y. Qiu, W. Li, F. Lao, G. Zhou, B. Sun, G. Xing, J. Dong, Y. Zhao, Z. Chai and C. Chen, *Biomaterials*, 2009, **30**, 3934–3945. [PMID: 19403166].
22 F. Antunes, E. Cadenas and U. T. Brunk, *Biochem. J.*, 2001, **356**, 549–555. [PMID: 11368784].
23 S. Eruslanov and E. Kusmartsev, *Methods Mol. Biol.*, 2010, **594**, 57–72. [PMID: 20072909].
24 R. C. Scaduto Jr and L. W. Grotyohann, *Biophys. J.*, 1999, **76**, 469–477. [PMID: 9876159].
25 C. Ferlini, S. Di Cesare, G. Rainaldi, W. Malorni, P. Samoggia, R. Biselli and A. Fattorossi, *Cytometry*, 1996, **24**, 106–115. [PMID: 8725659].
26 H. Liu, C. Zhang, Y. Tan, J. Wang, K. Wang, Y. Zhao, G. Jia, Y. Hou, S. Wang and J. Zhang, *J. Nanopart. Res.*, 2014, **16**, 2303.
27 C. R. Patra, S. S. Abdel Moneim, E. Wang, S. Dutta, S. Patra, M. Eshed, P. Mukherjee, A. Gedanken, V. H. Shah and D. Mukhopadhyay, *Toxicol. Appl. Pharmacol.*, 2009, **240**, 88–98. [PMID: 19616569].
28 J. Wang, C. Chen, B. Li, H. Yu, Y. Zhao, J. Sun, Y. Li, G. Xing, H. Yuan, J. Tang, Z. Chen, H. Meng, Y. Gao, C. Ye, Z. Chai, C. Zhu, B. Ma, X. Fang and L. Wan, *Biochem. Pharmacol.*, 2006, **71**, 872–881. [PMID: 16436273].
29 P. V. AshaRani, G. Low Kah Mun, M. P. Hande and S. Valiyaveettil, *ACS Nano*, 2009, **3**, 279–290. [PMID: 19236062].
30 R. Chen, Z. Huang, G. Chen, Y. Li, X. Chen, J. Chen and H. Zeng, *Int. J. Oncol.*, 2008, **32**, 861–867. [PMID: 18360713].
31 X. Jiang, R. Foldbjerg, T. Miclaus, L. Wang, R. Singh, Y. Hayashi, D. Sutherland, C. Chen, H. Autrup and C. Beer, *Toxicol. Lett.*, 2013, **222**, 55–63. [PMID: 23872614].
32 A. C. Johansson, H. Appelqvist, C. Nilsson, K. Kagedal, K. Roberg and K. Ollinger, *Apoptosis*, 2010, **15**, 527–540. [PMID: 20077016].
33 P. Boya and G. Kroemer, *Oncogene*, 2008, **27**, 6434–6451. [PMID: 18955971].
34 F. Antunes, E. Cadenas and U. T. Brunk, *Biochem. J.*, 2001, **356**, 549–555. [PMID: 11368784].
35 T. Sato, T. Machida, S. Takahashi, K. Murase, Y. Kawano, T. Hayashi, S. Iyama, K. Takada, K. Kuribayashi, Y. Sato, M. Kobune, R. Takimoto, T. Matsunaga, J. Kato and Y. Niitsu, *J. Immunol.*, 2008, **181**, 197–207. [PMID: 18566385].
36 M. Bras, B. Queenan and S. A. Susin, *Biochemistry*, 2005, **70**, 231–239. [PMID: 15807663].
37 Y. Jin, S. Chen, J. Duan, G. Jia and J. Zhang, *J. Inorg. Biochem.*, 2015, **146**, 28–36. [PMID: 25725393].
38 N. W. Werneburg, M. E. Guicciardi, S. F. Bronk and G. J. Gores, *Am. J. Physiol.: Gastrointest. Liver Physiol.*, 2002, **283**, G947–G956. [PMID:12223355].

 